J Mater Sci (2009) 44:4892–4899
DOI 10.1007/s10853-009-3747-6

Analysis of the high growth-rate transition in Al–Si eutectic solidification

T. Hosch · L. G. England · R. E. Napolitano

Received: 15 May 2009 / Accepted: 15 July 2009 / Published online: 30 July 2009

Abstract The local solidification conditions and mechanisms associated with the flake-to-fiber growth mode transition in Al–Si eutectic alloys are investigated here using Bridgman-type gradient-zone directional solidification. Resulting microstructures are examined through quantitative image analysis of two-dimensional sections and observation of deep-etched sections, showing three-dimensional microstructural features. Several microstructural parameters were investigated in an attempt to quantify this transition, and it was found that the particle aspect ratio is effective in objectively identifying the onset and completion velocity of the flake-to-fiber transition, whereas traditional spacing parameters are not effective indicators of the transition. For a thermal gradient of 7–14 K/mm, the transition was found to occur in two stages, appearing over velocity regimes from 0.10 to 0.50 mm/s and from 0.50 to 0.95 mm/s. The initial stage is dominated by in-plane plate breakup and rod formation within the plane of the plate, whereas the second stage is characterized by the onset of out-of-plane silicon rod growth, leading to the formation of an irregular fibrous structure. The boundary between the two stages is marked by widespread fibrous growth and the disappearance of the remnant flake structure, indicating a transition in the structural feature that governs the relevant diffusion length, from inter-flake spacing to inter-rod spacing.

T. Hosch · L. G. England · R. E. Napolitano (✉)
Department of Materials Science and Engineering,
Iowa State University, Ames, IA 50011, USA
e-mail: ralphn@iastate.edu

Introduction

The alloys based on the Al–Si eutectic system are among the most versatile for use in net-shape castings, offering an extensive range of properties suitable for a broad scope of engineering applications calling for high strength to weight ratio, good corrosion resistance, and excellent castability. While the intrinsic flake silicon morphology observed in conventional Al–Si castings imparts relatively poor mechanical properties, ductility and strength are significantly improved through modification practices, where the silicon flake structure is refined to a globular or fibrous morphology. Typical effects of modification on Al–Si cast alloys include a 50% improvement in tensile strength and a threefold improvement in ductility [1–5]. These enhanced properties are most commonly achieved through impurity modification [6–9], a practice where trace amounts of certain alloying additions (Na or Sr) induce a high density of {111} twins [7], giving rise to a microfaceted growth structure which allows local response to the evolving diffusion field and the formation of a fibrous morphology. However, in addition to the increased costs and recycling limitations, impurity modification is also associated with deleterious effects such as porosity, hot tearing, and poor surface finish [6, 9]. An alternative is to elicit a similar structural refinement and morphological transition through increased cooling rates, a practice known as quench modification [10, 11]. Quench modification yields a fine fibrous structure that is microscopically smooth, with a low density of incidental twins, clearly differentiating it from the microfaceted impurity-modified structure. However, the local interface conditions and mechanisms that lead to quench modification during solidification are not yet fully understood, thus limiting reliable prediction and effective employment of quench modification in certain casting

applications. More effective utilization of this growth mode transition for property enhancement requires better description of the transition itself in terms of quantitative microstructural parameters, enabling consistent identification of the transition and reliable determination of the prevailing local growth conditions.

To date, there have been many attempts to characterize the Al–Si eutectic microstructure. In particular, microstructural changes during impurity modification have been characterized with some success. Early methods of determining silicon modification level were based on manual microscopic assessment of the microstructure, which can be combined with thermal analysis observations to allow quick estimation of modification level [12]. Drawbacks to this method include a lack of objectivity when assessing modification level and a decrease in resolution of thermal analysis methods at higher cooling rates. Recently, computer image analysis technology has been applied to increase the objectivity and accuracy of these measurements. Jiang et al. [13] used a two-dimensional image analysis to objectively determine the Al–Si modification level with increasing Sr additions. Particle length, width, and perimeter were found to correlate well with changing levels of structure modification. Hernandez and Sokolowski [14] expanded this technique to work on hypereutectic alloys and also found particle perimeter to effectively differentiate modification level.

The microstructural changes associated with the quench modification transition have not been characterized as thoroughly as those associated with impurity modification. Average interphase spacing has been measured by several investigators over a range of solidification velocities, as shown in Table 1, but such spacing parameters contain only indirect morphological information and do not adequately reflect the changing growth mode behavior throughout the flake-to-fiber transition. Due to the lack of appropriate quantitative parameters that indicate the transition, previous estimates of the velocity for the quench modification transition (Table 2) are based on qualitative analysis of structure, and results vary significantly. With no established method

Table 1 Reported Al–Si eutectic growth parameters from length scale (λ) measurements

	Year	Gradient (K/mm)	Velocity (μm/s)	Measurement	A[a]	m[a]
Day and Hellawell [10]	1968	3–10	4–14	λ[b]	22	−0.56
Fredriksson et al. [16]	1973	30	4–400	λ[b]	46	−0.61
Toloui and Hellawell [17]	1976	0.7	20–400	$\lambda_{\parallel}, \lambda_A$	46	−0.41
		1.5	20–400	$\lambda_{\parallel}, \lambda_A$	35	−0.42
		4.5	20–400	$\lambda_{\parallel}, \lambda_A$	28	−0.43
		8	20–400	$\lambda_{\parallel}, \lambda_A$	25	−0.45
		15	20–400	$\lambda_{\parallel}, \lambda_A$	23	−0.48
Elliott and Glenister [18]	1980	0.8	5–170	λ[b]	26	−0.33
Atasoy [19]	1984	12	10–474	$\lambda_{\parallel}$	25	−0.34
Hogan and Song [20]	1987	11	10–200	$\lambda_{\parallel}$	23	−0.45
Liu et al. [21]	1990	9–11	5–200	$\lambda_{\parallel}$	25	−0.46
Magnin et al. [22]	1991	8	0.1–500	$\lambda_{\parallel}$[c]	34	−0.5
Khan and Elliott [23]	1996	12.2	28–875	$\lambda_{\parallel}, \lambda_A$	32	−0.47
		7.6	28–875	$\lambda_{\parallel}, \lambda_A$	30	−0.43
Wolczynski et al. [24]	1996	8	3–70	$\lambda_{\parallel}$	19	−0.50
		0.8	10–165	$\lambda_{\parallel}$	24	−0.30
Cuprys et al. [25]	2000	4	300–790	$\lambda_{\parallel}, \lambda_A$	22	−0.47
		10	300–790	$\lambda_{\parallel}, \lambda_A$	15	−0.4
Napolitano and England [15]	2004	7.5	10–1200	λ_A	37	−0.52
		7.5	10–1200	λ_L	56	−0.49
Guzik and Kopyczynski [26]	2006	10.5	0.3–11	$\lambda_{\parallel}$[d]	17	−0.35
Current study		7–14	10–2000	$\lambda_{\parallel}$	27	−0.53
		7–14	10–2000	λ_A	48	−0.55
		7–14	10–2000	λ_L	55	−0.52

[a] All parameters given as $\lambda = AV^m$

[b] Unspecified linear intercept method

[c] Selected eutectic regions for intercept analysis not restricted to areas where lamellae were strictly parallel

[d] Lines for spacing determination were drawn parallel to the growth interface

Table 2 Reported transition velocities

	Gradient (K/mm)	Velocity (μm/s)
Steen and Hellawell [27]	11	400–800
	23	160–200
Jenkinson and Hogan [8]	9-40	480–1000
Toloui and Hellawell [17]	8	800–1000
Atasoy [19]	12	395–570
Khan and Elliott [23]	8-12	505–807
Napolitano and England [15]	7.5	100–1000

for objective identification of the flake–fiber transition, processing-map boundaries indicating the conditions which give rise to flake or fibrous morphologies are not well defined, and growth-mode prediction based on local solidification parameters is not reliable. A preliminary analysis [15] verified that the flake-to-fiber transition occurs over a wide velocity range and suggested that new microstructural parameters may be able to indicate the transition. In the work presented here, we (i) quantitatively characterize the Al–Si microstructure over different velocities of solidification using a few selected microstructural parameters, and (ii) qualitatively analyze the process of quench modification to examine more closely the microstructural mechanisms associated with the growth-mode transition indicated by the quantitative measurements.

Experimental methods and findings

Alloy test specimens of an Al–13 wt%Si alloy were fabricated by vacuum-arc-melting the pure constituents (<10 ppm impurities) on a water-cooled copper hearth, casting into 8-mm billets, swaging to 5-mm diameter rods, and cutting to lengths of 300 mm.

Directional solidification experiments were performed in a Bridgman-type furnace over a range of velocities from 10 to 2000 μm/s. The temperature gradient during solidification was measured using a thermocouple embedded in a separate sample and ranged from 7 K/mm at 10 μm/s to 14 K/mm at 1000 μm/s. Test specimens were contained in an alumina tube of 5.5 mm inner diameter and 8.0 mm outer diameter. Samples were grown over a distance of 50 mm and then quenched to 25 °C in a water-cooled bath containing a Ga–In–Sn alloy. Cross sections were taken from each sample 10 mm behind the final quenched interface to obtain a representative eutectic structure and prepared for metallographic analysis. Characteristic microstructures observed over the range of velocities are shown in Fig. 1. Early stages of the flake-to-fiber transition can be seen at velocities as low as 20–50 μm/s, though the images suggest that the transition occurs primarily over the velocity range of 100 to 950 μm/s.

Specimens to be used for the determination of interflake spacing were polished and etched with a 2.5%HCl–1.5%HNO_3–1%HF reagent for 10–30 s for SEM analysis. Selected specimens were deep etched by suspending in an ultrasonic bath with the etchant for 1 h. Three conventional spacing metrics were determined from eutectic cross sections. The spacing between parallel flakes, $\lambda_{\parallel}$, was measured using intercept lines perpendicular to selected silicon flakes observed to be approximately parallel. The random line spacing, λ_L, was determined using intercept lines oriented randomly. An area-based spacing parameter, λ_A, was calculated as:

$$\lambda_A = \sqrt{A/N},$$

where N is the number of particles that are observed on a two-dimensional analysis area, A. A schematic demonstrating the parallel and random line spacing measurements is shown in Fig. 2. The conventional spacing parameter results are shown in Fig. 3 as a function of velocity. All spacing parameters closely followed a $\lambda^2 V = \text{constant}$ relationship.

The average particle aspect ratio was also used to characterize the silicon structure. This is defined as the ratio of the largest caliper dimension of a particle to the smallest dimension perpendicular to the maximum. The aspect ratio as a function of velocity is displayed in Fig. 4. The data show three distinct regimes marked by abrupt transitions in slope at the velocities 135 and 880 μm/s. These velocities bound the transition range, within which both flake and fiber morphologies are readily observed.

Analysis and discussion

Qualitative inspection of the microstructures shown in Fig. 1 reveals that the flake-to-fiber transition occurs gradually (with velocity) and in somewhat overlapping but distinct stages. In the lowest studied velocities of 10 and 20 μm/s, the microstructure consists of large silicon plates. The plate structure is generally unbroken, though there are isolated instances where individual plates or groups of plates have begun to break up. This is not entirely unexpected, given the inherently large variation in local spacings and solidification conditions of irregular eutectic alloys. In the 50 and 100 μm/s structures, there appears to be only slight if any deviation from the broad plate structure. Indeed, if one ignores scale, it is difficult to differentiate between the microstructures in this range, indicating the flake-to-fiber transition has not yet begun. However, a significant change is seen from 100 to 250 μm/s. At 250 μm/s,

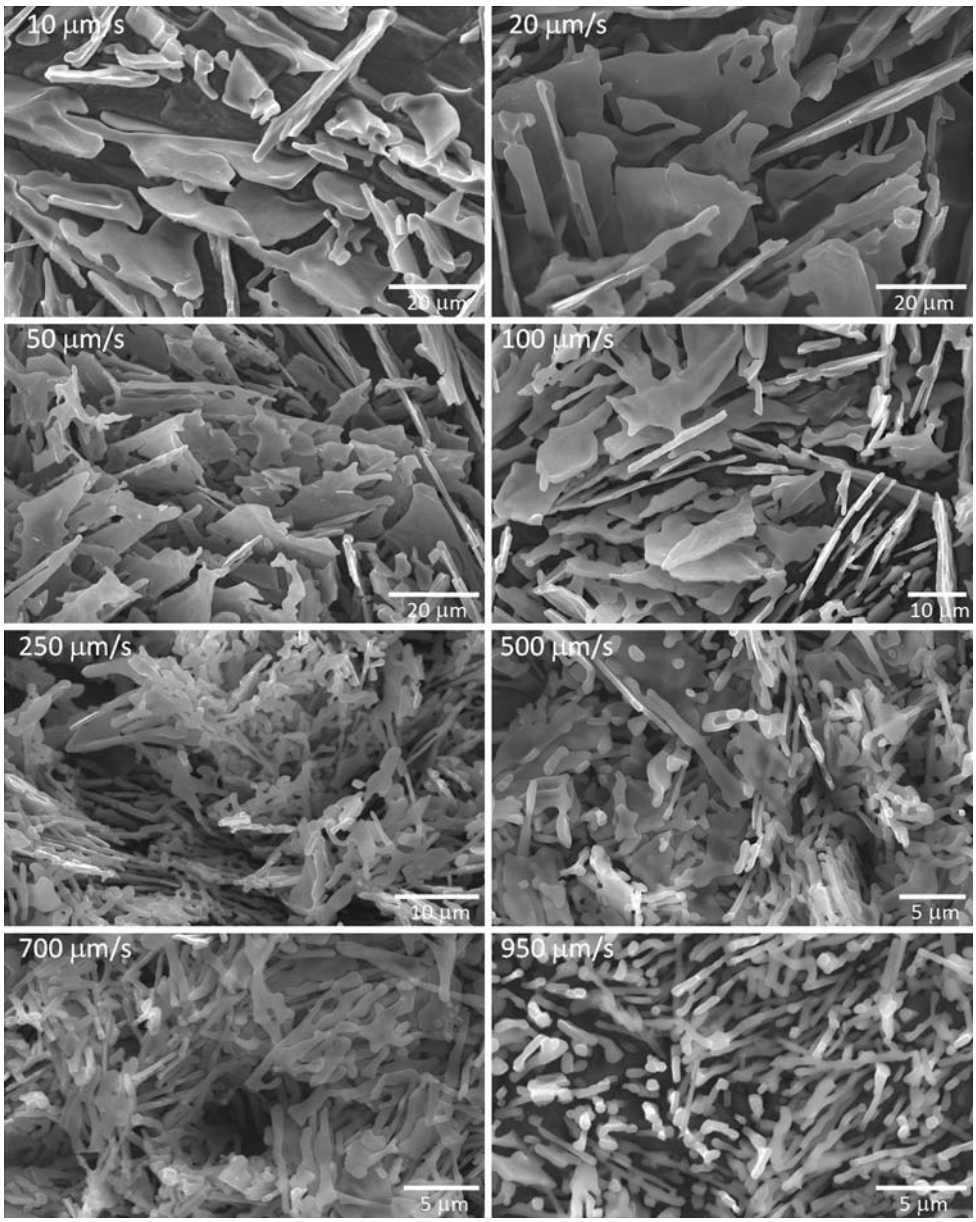

Fig. 1 Typical silicon morphology after directional solidification of an Al–Si eutectic alloy in a temperature gradient of 7–14 K/mm over a velocity range from 10 to 950 μm/s. The Al-rich phase has been chemically removed

the plate structure has degraded significantly, leaving a dispersion of skeletal plates and various rodlike structures within the plane of the plate, indicating the beginning of the flake-to-fiber transition. Another important event is noted at 500 μm/s. For the first time, out-of-plane rod growth is seen. Several examples of rods growing out of flat plate faces are evident, as well as instances of extended rod growth mixed with the eroding plate structure. Whereas at 250 μm/s rods were beginning to evolve within the plane of the plate, by 500 μm/s growth has become possible outside of the plane of the plate as well. The conversion to rod-dominated growth continues through 700 μm/s, and is generally complete by 950 μm/s. The microstructure at 950 μm/s contains little to no remnant plate structure and is instead dominated by rod growth which is weakly aligned with the growth direction. From these observations, the flake-to-fiber transition is said to occur in two stages: an initial stage which begins between the velocities of 100 and 250 μm/s and involves breakup of the broad plate structure and in-plane rod formation, and a final stage which begins near the velocity 500 μm/s and involves the initiation of out-of-plane rod growth and continues until the transition to rod-dominated growth is complete by 950 μm/s.

Evolving microstructural features of the eutectic with increasing velocity are representative of the intrinsic growth mechanisms being selected. Higher-magnification images of the evolving eutectic structures are shown in Fig. 5. The sequence of morphologies observed upon growth from 20 to 250 μm/s suggests that the transition involves a selection phenomenon based on the hierarchy of

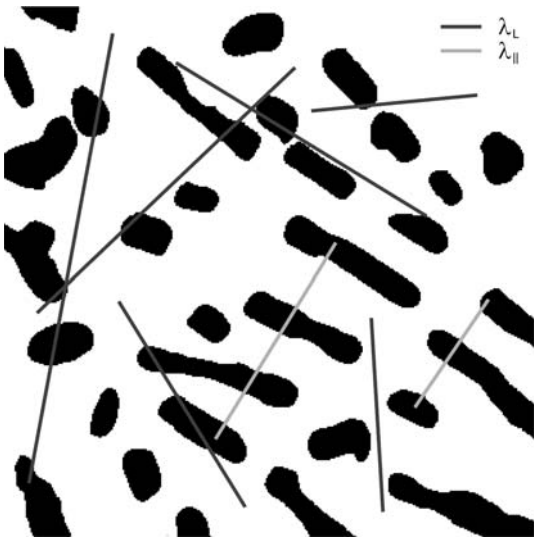

Fig. 2 Schematic demonstrating the calculation of the parallel and random line spacing measurements. The $\lambda_{\|}$ measurement is determined by drawing lines perpendicular to parallel silicon plates while the λ_L measurement involves the generation of random lines over the eutectic area

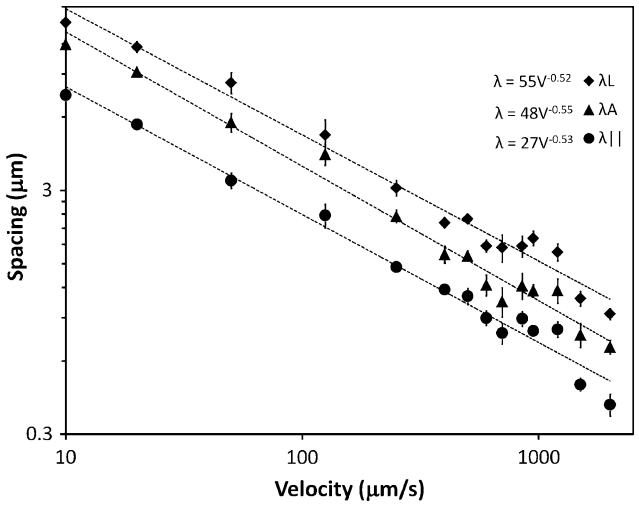

Fig. 3 Graph of three different spacing parameters. The λ_L measurement reflects the average spacing considering all possible line orientations. The $\lambda_{\|}$ measurement indicates the average spacing perpendicular to parallel silicon particles. The λ_A measurement is effectively an inverse particle density function, indicating that particles become more numerous within a constant volume at high velocities. Error bars represent the 95% confidence interval of the mean

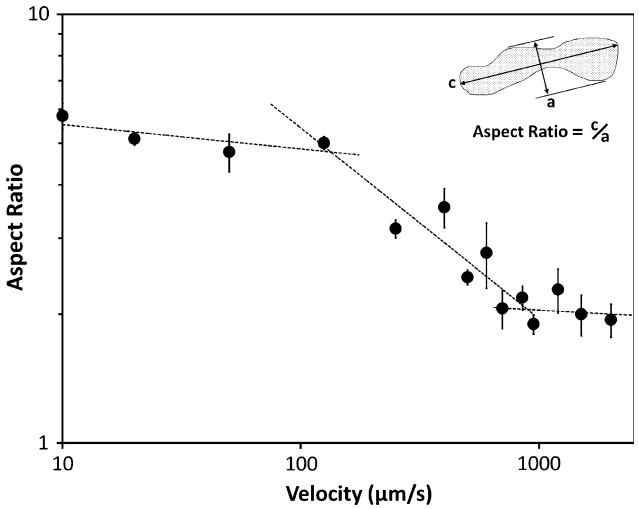

Fig. 4 Graph of the average particle aspect ratio for the range of velocities studied. The aspect ratio displays distinct transition points near 135 and 880 μm/s, which are near the visually observed onset and conclusion velocities of the flake to fiber transition. Error bars represent the 95% confidence interval of the mean

interfacial properties. In particular, it is important to note the manner of plate breakup at these velocities. The appearance of gaps, holes, and other convoluted formations within otherwise well-defined plate structures indicates that, while growth is still generally confined to within the {111} plane of the plate, multiple in-plane growth directions are operative. In effect, growth is becoming more nearly isotropic in the plane of the plate. This progression leads to the development of increasingly thin skeletal plates and, ultimately, the formation of rodlike structures within the plane of the plate. Additionally, it becomes apparent at 500 μm/s that out-of-plane growth sites are active at select locations in the structure. For example, it is seen in Fig. 5 that silicon protrusions begin to form on plate faces by 500 μm/s and grow approximately perpendicular to the plate face. These isolated instances could be a result of locally higher eutectic spacings and subsequently increased local solute gradient. Silicon protrusion formation occurs along with an increased incidence of extended fibrous growth, both of which dominate the microstructure by 950 μm/s, as shown in Figs. 1 and 5. A more extensive example of protrusion formation is shown in Fig. 6. Here, silicon fingers grow out of plate faces at a defined spacing. As the remnant plate structure disappears in the eutectic, it becomes difficult to determine whether predominant rod growth is truly three-dimensional in nature or remains confined within the {111} silicon planes. However, with substantial out-of-plane protrusion formation on crystal facets at velocities as low as 500 μm/s, it is reasonable to assert that localized morphological instability plays a vital role in the onset and completion of the flake-to-fiber transition.

If the operative flake-to-fiber transition mechanism involves the activation of additional growth sites with increasing solidification velocity, then one would expect the predominant silicon fiber growth axis to change with velocity as well. Favored in-plane growth directions would

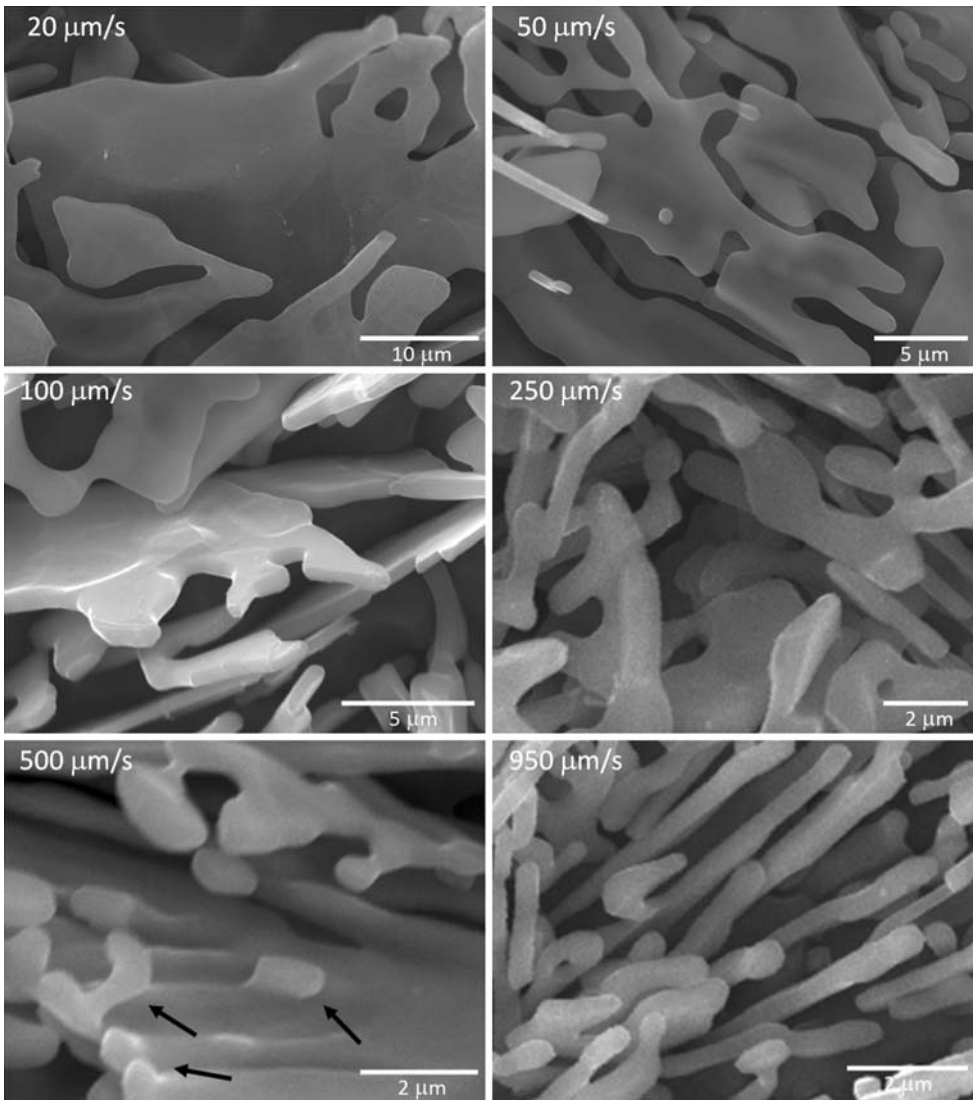

Fig. 5 Details of the quench modification process in an Al–13 wt%Si alloy. At velocities from 10 to 250 μm/s the transition is evident in the breakup of plates, with rodlike structures evolving within the envelope of the plate. At higher velocities, the next stage of the transition becomes evident as out-of-plane rod growth begins around 500 μm/s (*arrows*) and a shift to rod dominance occurs by 950 μm/s

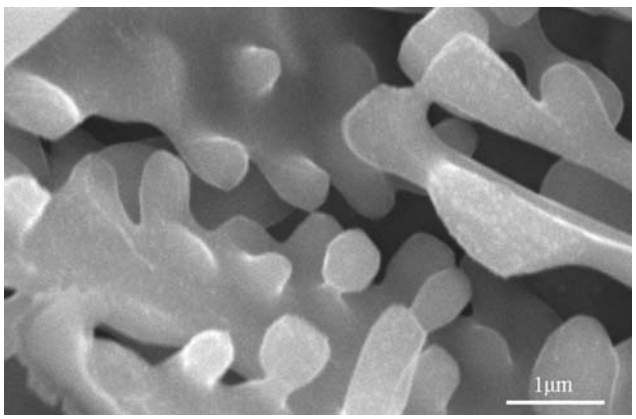

Fig. 6 Occurrence of morphological instability of plate faces in a sample grown at 950 μm/s

be prevalent at low velocities, whereas additional in-plane and ultimately out-of-plane fibrous growth directions would become common with increasing velocity. The crystallographic orientation of quench-modified silicon fibers has been studied to some extent. At lower velocities, Lu and Hellawell [11] and Shamsuzzoha and Hogan [28] found a tendency for plates to elongate in ⟨211⟩ directions and Lu and Hellawell similarly noted that quench-modified fibers assumed a general growth direction of approximately ⟨211⟩. Steen and Hellawell [27] observed the occurrence of ⟨211⟩ fiber growth, but reported the most common growth direction was ⟨110⟩. Jenkinson and Hogan [8], meanwhile, found the dominant fiber axis to be consistently ⟨100⟩. While a relationship between velocity and fiber orientation was not reported by these authors, the variable orientation results support the possibility of fiber growth in multiple directions with a predominant growth direction that evolves with changing velocity as is consistent with the present findings. Furthermore, the observation of dominant ⟨100⟩ growth in the study by Jenkinson and Hogan is significant in that it represents an out-of-plane

growth direction, proving that out-of-plane growth may increase to the extent that it dominates the quench-modified microstructure.

The evolution of silicon morphology with increasing velocity is governed by distinct levels of silicon interfacial energy. At low velocities (and low undercoolings), the faceted, microscopically smooth morphology of flake silicon is preferred [29]. Increased undercooling at higher velocities precipitates the activiation of additional in-plane growth directions leading to the formation of in-plane rod structures, and, at the highest velocities, the activation of out-of-plane growth directions in select locations leads to the formation of rod-type silicon protrusions approximately perpendicular to plate faces. The appearance of these fibrous growth structures eventually dominates the eutectic structure, completing the flake-to-fiber transition. It should be noted that an earlier study by Khan and Elliott [23] reported a discrete decrease in undercooling above 500 μm/s. While this result does not appear to be consistent with the present observation of a gradual flake-to-fiber transition occurring over a wide range of velocities beginning below 250 μm/s, it may be indicative of the onset of out-of-plane growth defining the beginning of the second stage of the transition. The erosion of the plate structure and subsequent onset of out-of-plane growth will contribute to a change in the intrinsic length scale. While the evident microstructural morphology changes gradually, it is possible that a relatively abrupt change in the dominant diffusion length scale from interplate to interfiber distances corresponds to a sudden decrease in local undercooling.

The conventional spacing parameters examined closely follow a $\lambda^2 V =$ constant relationship and differ only by a constant multiplier, as shown in Fig. 3. As expected, the parameters do not indicate the flake-to-fiber transition in any way and, hence, do not reflect the evolving silicon microstructure. The spread in spacing values between different parameters is similar to the spread in previously reported spacing results. Due to the spread in magnitude of the results, the degree to which any of the spacing parameters approximate the true average inter-fiber diffusion distance during solidification is in doubt. Each of the three parameters has its drawbacks. The subjective, selective nature of the $\lambda_{\|}$ measurement suggests it is not an accurate representation of the whole microstructure. The λ_A method suffers from the difficulty of determining which particles are separate, especially in the flake structure. Finally, the λ_L results will be biased upwards due to a reliance on random alignments that do not coincide with the minimum distance between two adjacent particles. Furthermore, all the spacing parameters employed suffer from the limitations of the two-dimensional microstructure projections they are based on.

Unlike the spacing parameters, the aspect ratio data shown in Fig. 4 indicate a transition with changing velocity. The initial abrupt change in the slope of the graph occurs at about 135 μm/s, indicating the data may be reflecting the onset of the flake-to-fiber transition, which was determined to occur between 100 and 250 μm/s. This behavior is reasonable, given that the transition involves the conversion of high aspect ratio broad flakes to low aspect ratio skeletal plates and rod structures. Furthermore, the data show a second and opposite slope change near 880 μm/s, which is attributed to the end of the flake-to-fiber transition, where the conversion to rods is largely complete and the aspect ratio ceases to drop. The transitions shown by the aspect ratio data are useful in that they define objective measures for determining the onset and completion velocities of the flake-to-fiber transition, allowing consistent identification of the transition.

Conclusions

1. Qualitative observations suggest the flake-to-fiber transition occurs within two overlapping but distinct intervals, defined below.
   a. 100–500 μm/s: This stage is characterized by a rapid increase in the in-plane breakup of broad silicon plates to skeletal plate and rodlike structures. This occurrence signifies the activation of additional in-plane growth directions due to increased undercooling.
   b. 500–950 μm/s: This stage begins with the onset of out-of-plane silicon growth, leading to fibrous rod structures and three-dimensional growth. There is also a marked increase in incidences of silicon morphological instabilities growing out of sheer plate faces. This stage terminates with the completion of the flake-to-fiber transition.

   Furthermore, despite descriptions of flake to fiber onset and completion velocities, a range of silicon growth mechanisms are present at all velocities studied (10–2000 μm/s), and the flake-to-fiber transition, as reported, simply reflects those velocities at which the dominant growth mechanism changes. Al–Si eutectic growth may, therefore, be more aptly described with a model that incorporates flake, fiber, and other mechanisms of growth at all velocities in this range.
2. The appearance of out-of-plane silicon protrusions midway through the flake-to-fiber transition suggests that the occurrence of three-dimensional out-of-plane silicon growth is vital to the formation of the modified fibrous microstructure. The flake to fiber transition may then be said to involve a transition from the primarily two-dimensional growth of eutectic silicon as bulky plates at low velocities to primarily three-dimensional

growth of eutectic silicon as globular fibers at high velocities. A salient feature of this transformation is the change from flake-dominated diffusion distances to fiber-dominated diffusion distances.

3. None of the conventional spacing parameters are effective in indicating the flake-to-fiber transition. Therefore, more descriptive parameters must be included in any model meant to describe the microstructure and growth modes present in the silicon eutectic.
4. The relationship between aver age particle aspect ratio and solidification velocity objectively defines a velocity for both the beginning and end of the flake-to-fiber transition. Stages of the transition are indicated by abrupt changes in the slope of the aspect ratio versus velocity relationship. In this manner, the beginning of the flake-to-fiber transition in the Al–Si eutectic alloy was determined to be 135 μm/s, and the end was determined to be 880 μm/s. While this range compares well with the qualitative assessment based on morphology, it is a more objective measure of the flake-to-fiber transition and, therefore, more suitable for use in the prediction of solidification microstructure.

Acknowledgements This study was made possible by support from the National Science Foundation (NSF), Division of Materials Research, under Award no. 0237566. The authors would also like to thank P. Matlage for experimental assistance.

References

1. Fat-Halla N (1987) J Mater Sci 22(3):1013. doi:10.1007/BF01103544
2. Fat-Halla N (1989) J Mater Sci 24(7):2488. doi:10.1007/BF01174517
3. Hafiz MF, Fat-Halla NK, Moshref SB (1990) Zeitschrift für Metallkunde 81(1):70
4. Hafiz M, Kobayashi T (1994) Scripta Metallurgica et Materialia 31(6):701
5. Zuo M, Liu XF, Sun QQ (2009) J Mater Sci 44(8):1952. doi:10.1007/s10853-009-3287-0
6. Garat M, Laslaz G, Jacob S, Meyer P, Guerin PH, Adam R (1992) Trans Am Foundrymen's Soc 100:821
7. Lu SZ, Hellawell A (1987) Metall Trans A 18A(10):1721
8. Jenkinson DC, Hogan LM (1975) J Cryst Growth 28(2):187
9. Dahle AK, Nogita K, McDonald SD, Dinnis C, Lu L (2005) Mater Sci Eng A 413–414:243
10. Day MG, Hellawell A (1968) Proc R Soc Math Phys Eng Sci 305(1483):473
11. Lu SZ, Hellawell A (1985) J Cryst Growth 73(2):316
12. Tenekedjiev N, Gruzleski JE (1991) Trans Am Foundry Soc 99:1
13. Jiang H, Sokolowski JH, Djurdjevic MB, Evans WJ (2000) Trans Am Foundry Soc 108:505
14. Hernandez FCR, Sokolowski JH (2005) J Met 57
15. Napolitano RE, England LG (2004) Solidification of aluminum alloys. TMS, Warrendale, PA
16. Fredriksson H, Hillert M, Lange N (1973) J Inst Met 101:285
17. Toloui B, Hellawell A (1976) Acta Metall 24(6):565
18. Elliott R, Glenister SMD (1980) Acta Metall 28(11):1489
19. Atasoy O (1984) Aluminium 60(4):275
20. Hogan LM, Song H (1987) Metall Trans A 18A(4):707
21. Liu J, Zhou Y, Shang B (1990) Acta Metallurgica et Materialia 38(7):1321
22. Magnin P, Mason JT, Trivedi R (1991) Acta Metallurgica et Materialia 39(4):469
23. Khan S, Elliott R (1996) J Mater Sci 31(14):3731. doi:10.1007/BF00352787
24. Wolczynski W, Billia B, Rabczak K (1996) Mater Sci Forum 215:323
25. Cuprys R, Major B, Wolczynski W (2000) Mater Sci Forum 329:161
26. Guzik E, Kopyczynski D (2006) Metall Mater Trans A 37A(10):3057
27. Steen HAH, Hellawell A (1972) Acta Metall 20(3):363
28. Shamsuzzoha M, Hogan LM (1986) J Cryst Growth 76(2):429
29. Li L, Zhang YD, Esling C, Zhao ZH, Zuo YB, Zhang HT, Cui JZ (2009) J Mater Sci 44(4):1063. doi:10.1007/s10853-008-3158-0